AIAA JOURNAL
Vol. 47, No. 7, July 2009

Planar Velocimetry of a Fin Trailing Vortex in Subsonic Compressible Flow

Steven J. Beresh,* John F. Henfling,† and Russell W. Spillers‡
Sandia National Laboratories, Albuquerque, New Mexico 87185

DOI: 10.2514/1.42097

A subscale experiment has studied the trailing vortex shed from a tapered fin installed on a wind-tunnel wall to represent missile configurations. Stereoscopic particle image velocimetry data have been acquired for several locations downstream of the fin and at different fin angles of attack. The vortex's tangential velocity decays with downstream distance while its radius increases, but the vortex core circulation remains constant. Circulation and tangential velocity rise greatly for increased fin angle of attack, whereas the radius remains approximately constant or slightly decreasing. The vortex axial velocity is always a deficit, whose magnitude diminishes with downstream distance and smaller angle of attack. No variation with Mach number can be discerned in the normalized velocity data. Vortex roll up is largely complete by about four root chord lengths downstream of the fin trailing edge; before this point, the vortex is asymmetric in the tangential velocity but the core radius stays nearly uniform. Vortical rotation draws low-speed turbulent fluid from the wind-tunnel wall boundary layer and the fin wake toward the vortex core, which appears to hasten vortex decay and produce a larger axial velocity deficit than expected. Self-similarity of the vortex is established even while it is still rolling up.

Introduction

MODERN precision-guided air-delivered weapons generally combine the presence of fins with strakes or canards. Consequently, the tip vortices shed from the upstream control surfaces propagate downstream where they can interact with subsequent control surfaces and dramatically alter the expected performance, an interaction for which neither the knowledge base nor the predictive modeling is adequately dependable. Such fin–wake interactions often are addressed by conducting wind-tunnel tests on each specific flight configuration, then deriving aerodynamic models that can be used by the guidance system. Clearly, this inefficient approach can be improved by complementing it with reliable predictive tools to reduce the testing requirements, but common engineering-level methods are hampered by the challenge of accurately predicting the vortices shed by control surfaces across a wide range of flow conditions and geometric variations. Higher-fidelity computational fluid dynamics analyses can provide superior results if they employ underlying models that have been suitably developed and validated against reliable experimental data for the regime in which they will be applied. Although numerous wind-tunnel tests have been conducted on finned missile configurations, such data typically contain only integrated force measurements rather than flowfield measurements of the vortices themselves, and furthermore may not be available for public consumption.

A considerable body of flowfield data has been acquired of trailing vortices generated by lifting surfaces and is readily available in the open literature, but the preponderance of it concerns aircraft wings rather than the low-aspect-ratio control surfaces common to munitions. The subject has been studied for sufficiently long that a number of reviews are available [1–4], but in none are trailing vortices from fin geometries explicitly discussed. In [5,6] are well-known examples of wind-tunnel studies of tip vortices produced by scale models of actual aircraft, whereas [7–12] examined the tip vortices from simple wings constructed from classical airfoil shapes. The general goals of these works and others have been to identify the structure of the trailing vortex as a function of the wing geometry and flow parameters and additionally to establish similarity laws where feasible, and much of the resulting knowledge is useful in understanding the analogous fin vortices. Few studies, however, have addressed vortices generated by shapes more akin to missile fins. Shekarriz et al. [13] and Bridges et al. [14] examined the stubby sail found on a submarine body, Stinebring et al. [15] looked at a hydrofoil with an interest toward cavitation, and both Chow et al. [16] and Ramaprian and Zheng [17] investigated low-aspect-ratio versions of classical airfoil shapes; in all these cases, the authors noted an effect upon the trailing vortex by the proximity of the wall upon which the lifting surface was mounted, in contrast to the findings from aircraft wings. None of the aforementioned studies concern compressible flows, which are of interest to designers of bombs and missiles, and apparently the only modern comparable studies are the supersonic double-wedge shapes of Smart et al. [18] and Wang and Sforza [19], although Milanovic and Kalkhoran [20] performed the related investigation of the trailing vortices from a supersonic delta wing.

To provide data tailored towards the low-aspect-ratio control surfaces integral to fin–wake interactions, an experimental program in Sandia's Trisonic Wind Tunnel (TWT) has been conducted to study the vortex shed from a fin installed on a wall of the tunnel. The wind-tunnel wall represents the surface of a hypothetical flight vehicle rather than employing a traditional sting-mounted model of a missile body, so that a reasonably sized flowfield may be produced in a smaller facility. The present report discusses only the portion of the data set gathered with a single fin placed into the wind tunnel and is, therefore, focused upon the behavior of the trailing vortex. Concerning the broader research program, it is assumed that the same vortex shed from the upstream fin would impinge upon a second fin placed downstream of the first, a proposition tested in Beresh et al. [21] and found to be well supported. Data herein are acquired using stereoscopic particle image velocimetry (PIV) in the flowfield cross plane to directly measure the trailing vortex and the wake of the fin. Such a data set can be used to develop and validate computational models within the flight regime of interest to Sandia for precision-guidance flight hardware.

Presented as Paper 4179 at the 38th AIAA Fluid Dynamics Conference, Seattle, WA, 23–26 June 2008; received 9 November 2008; revision received 25 February 2009; accepted for publication 1 March 2009.

*Principal Member of the Technical Staff, Engineering Sciences Center, PO Box 5800, Mailstop 0825, Phone: (505) 844-4618; sjberes@sandia.gov. Associate Fellow AIAA.
†Distinguished Technologist. Member AIAA.
‡Senior Technologist.

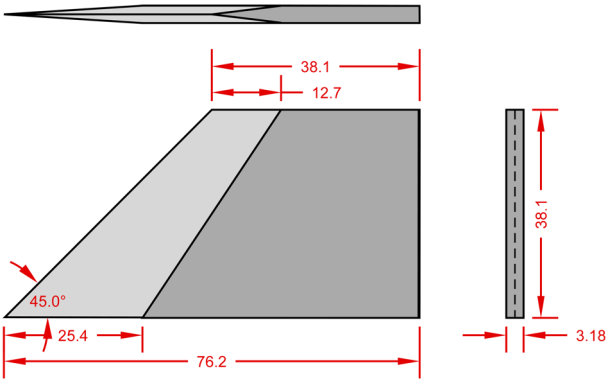

Fig. 1 Sketch of the fin geometry. Dimensions in mm.

Experimental Apparatus

Trisonic Wind Tunnel

Experiments were performed in the TWT, which is a blowdown-to-atmosphere facility using air as the test gas through a 305×305 mm^2 (12×12 in.^{2}) rectangular test section enclosed within a pressurized plenum. A solid-wall transonic test section was used for the present work rather than the traditional ventilated version because it offers reasonable optical access, a flat plate upon which models may be mounted, and computationally tractable boundary conditions for comparison of experimental data and numerical simulations. The use of a solid-wall test section limits the Mach number range of the flowfield, but this was considered an acceptable compromise.

Fin Hardware

The fin employed in the present study is drawn in Fig. 1, designed as a generic representation of the various fin geometries that could be found on real-world systems. Based upon a trapezoidal planform, the leading edge sweep is 45 deg, the fin root chord 76.2 mm (3 in.), the fin span 38.1 mm (1.5 in.), and its thickness 3.18 mm (0.125 in.). This size allows a sufficient downstream extent of the fin wake to be surveyed within the test section length. The sharp leading edge has a taper that terminates at a length of 1/3 the chord, and the trailing edge and fin tip are both square cut. The fin passes through the test section wall using a hub-and-pin system and attaches to a rotary mount that can be set to discrete angles of attack ranging from −5 to +10 deg in 1 deg increments, pinned in place to tightly toleranced positions to promote repeatability. The center of rotation is the midpoint of the fin root. A gap of 1.5 mm (0.06 in.) exists between the root of the fin and the wind-tunnel wall. The axial position of the fin is adjustable within a range of 457 mm (18.0 in.) using a series of interchangeable sliding mounting blocks within a rail cut into the test section wall. The fin was fabricated from stainless steel to guard against aeroelastic deformation and black oxide coated to reduce background light scatter for the PIV measurements.

Particle Image Velocimetry System

The PIV laser sheet configuration for the fin vortex measurements in the TWT is shown in Fig. 2, in which stereoscopic PIV is used to obtain all three velocity components in the wind-tunnel cross plane. The laser sheet was aligned normal to the wind-tunnel axis and positioned to the midpoint of the test section side-wall window. The coordinate system is selected such that the u component lies in the streamwise direction and the v component is in the vertical direction, positive away from the top wall; the w component is chosen for a right-handed coordinate system. The origin is located at the trailing edge of the fin root in its zero angle-of-attack position, regardless of its position along the test section axis. A positive fin angle of attack rotates the fin counterclockwise in the x-z plane.

The light source was a frequency-doubled dual-cavity Nd:YAG laser (Spectra Physics PIV-400) that produced about 400 mJ per beam. The beams were formed into coplanar sheets and directed into the test section from beneath the wind tunnel. To limit the particle dropout arising from the alignment of the freestream direction of the wind tunnel with the out-of-plane motion through the laser sheet, a relatively thick laser sheet of about 2 mm and brief time between pulses of 1.40 μs were employed.

The TWT is seeded by a thermal smoke generator (Corona Vi-Count 5000) that produces a large quantity of particles typically 0.2–0.3 μm in diameter from a mineral oil base. Particles are delivered to the TWT's stagnation chamber upstream of the flow conditioning section. A posteriori analysis of the data presented subsequently derives a Stokes number on the order of 0.01, which indicates the particles are sufficiently small that they rapidly attain the local velocity and avoid particle lag biases even in the presence of velocity gradients due to the fin tip vortex [22,23]. Particle ejection from the vortex core was found not to be a problem.

Scattered laser light was collected by interline-transfer charge-coupled device cameras (Redlake MegaPlus ES4.0/E) with a resolution of 2048×2048 pixels digitized at 8 bits. The two cameras were equipped with 200 mm lenses mounted on Scheimpflug platforms to create an oblique focal plane aligned with the laser sheet. Both cameras looked through the same window, viewing the laser sheet from opposite directions, each at an angle of 57 deg to the laser

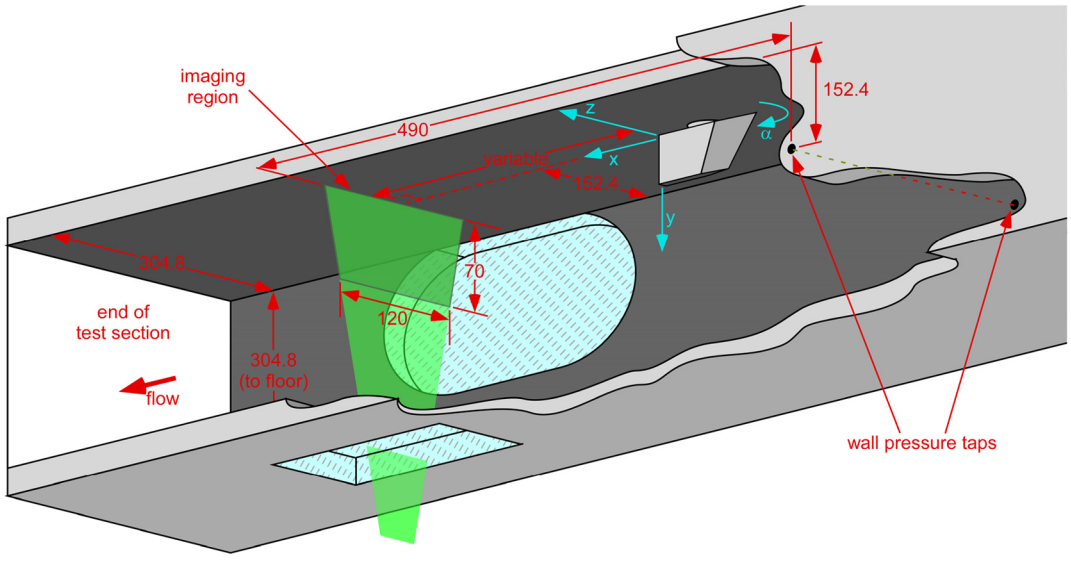

Fig. 2 Schematic of the PIV cross-plane configuration, looking downstream from below the test section. Flow from right to left. Dimensions in mm. Not to scale.

sheet normal. Limited optical access prevents meaningful movement of the cross-plane location upstream or downstream; thus all data have been acquired at a single position within the test section. Different stations with respect to the fin were achieved by moving the fin's location. Stereoscopic camera calibrations used the distorted sheet procedure described by Soloff et al. [24].

Data were processed using LaVision's DaVis v7.1 in two different ways, one in which image pairs were interrogated for greater precision at the expense of spatial resolution by using a 64×64 pixel window employing a two-pass adaptive correlation to account for the local particle displacement. Alternatively, the 64×64 pixel window was used as a first pass leading to two additional adaptive passes with a 32×32 pixel interrogation window, but these results are considerably noisier and were employed only for conditions in which large quantities of data were acquired to average out the random correlation noise. In either case, a 50% overlap in the interrogation windows was used as well to oversample the velocity fields. The spatial resolution varies across the image due to the oblique camera view, yielding about 4 mm horizontally and 2 mm vertically when measured at the wind-tunnel centerline for 64×64 pixel windows, and half this for 32×32 pixel windows. The software incorporates image deformation based upon local velocity gradients, using a bilinear interpolation scheme to warp the images. The resulting vector fields were validated based upon signal-to-noise ratio, nearest-neighbor comparisons, and allowable velocity range. The valid vector rate exceeds 98% for 64×64 pixel windows and 85% for 32×32 pixel windows, falling insignificantly in the vortex core.

Experimental Conditions

Testing conditions have been selected to represent a portion of the range flown by transonic vehicles that may incorporate precision-guidance capabilities. The freestream Mach numbers are $M_\infty = 0.5$, 0.6, 0.7, and 0.8 with the wind-tunnel stagnation pressure P_0 set to yield a test section static pressure $p_w = 101$ kPa (14.7 psia); this yields unit Reynolds numbers of 11×10^6 m^{-1}, 14×10^6 m^{-1}, 16×10^6 m^{-1}, and 19×10^6 m^{-1}, respectively. The wind-tunnel air supply is heated in the storage tanks but not temperature-controlled subsequent to this; therefore, the freestream stagnation temperature T_0 is subject to minor variation from 316 to 328 K (108–130°F).

The wall pressure p_w was measured from the mean of two static pressure taps located on the wind-tunnel side walls 490 mm upstream of the laser sheet location, as seen in Fig. 2. M_∞ and the freestream velocity U_∞ were calculated isentropically from the ratio p_w/P_0 and the stagnation temperature T_0. The freestream Mach number rises with downstream distance due to boundary-layer growth on the wind-tunnel walls in the constant-area cross section; hence, the actual Mach number at the fin location or laser sheet position will be greater than the nominal value established for the flow. To determine the local value, a series of pressure taps were installed in one side wall of the test section and recorded during every wind-tunnel run. The greatest rise occurs at Mach 0.8, where an increase to Mach 0.834 is observed at the laser sheet position.

The 99%-velocity boundary-layer thickness has been measured as 15.4 ± 0.4 mm (0.61 ± 0.02 in.) from PIV data acquired in the streamwise plane at $M_\infty = 0.8$ [25]. This measurement was made on the wind-tunnel centerline at the same downstream position as the cross-plane laser sheet. The ratio of boundary-layer thickness to fin height is similar to those predicted for vehicles of interest to Sandia.

Results and Discussion

Velocity Fields

Mean velocity data are shown in Fig. 3 for $M_\infty = 0.8$ at four angles of attack of the single fin, $\alpha = 2$, 5, 7, and 10 deg. The fin was mounted as far upstream in the wind tunnel as possible, thereby placing the PIV measurement location at a distance of $x/c = 4.18$ from the trailing edge of the fin, where c is the fin root chord. In-plane velocities are displayed as vectors superposed upon a contour plot of the out-of-plane (streamwise) velocities, with the vectors subsampled by a factor of two in each direction for visual clarity. The axes have been normalized to the fin root chord c and velocities by the freestream velocity as determined by the PIV data. All data are plotted on a common scale. The data of Fig. 3 were calculated using 64×64 pixel interrogation windows and averaged from 1200 individual realizations acquired over eight wind-tunnel runs for each case; superior spatial resolution is achieved using 32×32 pixel interrogation windows but this level of detail cannot suitably be displayed in plots such as these.

The uncertainty of the PIV measurements can be separated into precision and bias components. Determining the precision error is straightforward by analyzing repeated wind-tunnel runs for the $M_\infty = 0.8$, $\alpha = 10$ deg, $x/c = 4.18$ test conditions, from which the precision uncertainty is found to be about ± 2 m/s in each velocity component when using 64×64 pixel windows, including repeatability of the tunnel conditions from one run to another. Estimating the bias error due to the camera calibration (i.e., registration error) is more challenging. The calibration bias was found by reinstating the calibration target into the measurement location and traversing it a known distance in two dimensions corresponding to the expected particle motion in the time between laser pulses, then processing the resulting images as if they were PIV data. Bias values were found from the deviation of the measured translation with the actual motion, yielding a bias of about 4 m/s, which is at the limit of accuracy of positioning and translating the calibration target. The total uncertainty for 64×64 pixel windows, then, is about ± 5 m/s, equating to $\pm 0.02 U_\infty$, in each velocity component. However, when data are normalized by U_∞, the bias error largely cancels itself and the uncertainty in u/U_∞ diminishes to about ± 0.01.

Figure 3 (in particular Figs. 3c and 3d) shows that the fin tip vortex is clearly visualized, both by the in-plane rotation and the out-of-plane streamwise velocity deficit. As the angle of attack is increased, the strength of the vortex increases markedly, seen in the magnitudes of both the in-plane velocity vectors and the streamwise velocity deficit. A close study of Fig. 3 shows that the vortex position moves laterally farther from the centerline as α is increased, though it remains at a height roughly corresponding to the position of the fin tip. This lateral displacement exceeds the distance purely associated with the location of the fin trailing edge due to the fin cant. The fin tip vortex itself is analogous to the well-known aircraft wing tip vortices. The same characteristic structure is observed here, including the presence of a primary vortex core with a thin vortex sheet continuing to spiral around the core (in the present case, additionally lifting the wall boundary layer) and the prominence of axial flow within the vortex core.

The Mach number effect upon the fin trailing vortex was examined at $M_\infty = 0.5$, 0.6, 0.7, and 0.8. When appropriately normalized, no difference can be discerned between the four Mach numbers tested, and hence the figures are omitted. Measurement of derived quantities such as the vortex circulation, position, and size (see the following) quantitatively support this observation.

The downstream evolution of the vortex was studied by acquiring PIV data at the same station within the tunnel, as discussed earlier, but shifting the fin closer to the laser sheet. Figure 4 plots the velocity data at $\alpha = 10$ deg at positions $x/c = 0.51$, 1.18, and 2.18; the corresponding data at $x/c = 4.18$ is that of Fig. 3d. Note that the contour scale changes with each plot. A gradual decrease is evident in the magnitude of the in-plane velocities associated with the vortical rotation as well as the streamwise velocity deficit with downstream distance, accompanied by an apparent increase in vortex size.

Vortex Meander

It has been well established by past investigations that trailing vortices exhibit a low-frequency meander (alternatively termed "wander") in wind tunnels, in which a random lateral drift of the vortex core about a mean point is observed at frequencies much lower than those associated with turbulent motion [10,13,26–34]. This phenomenon typically is attributed to wind-tunnel freestream turbulence and therefore is considered an experimental artifact not found in flight conditions [10,26,27,33]. Conversely, Rokhsaz et al. [31] present data suggesting a cause other than freestream turbulence

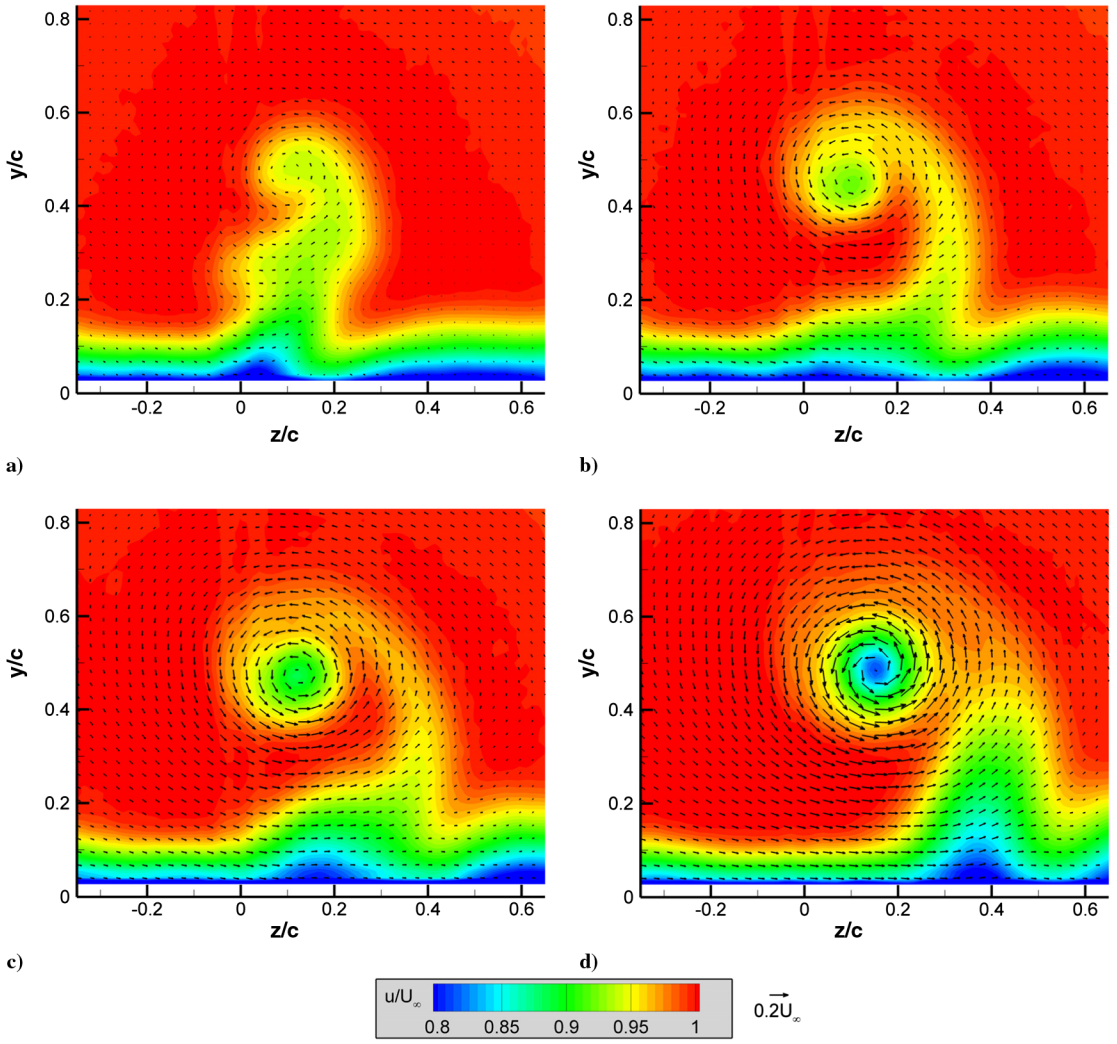

Fig. 3 Mean velocity fields at $M_\infty = 0.8$ at a distance of $x/c = 4.18$ from the trailing edge of the fin. a) $\alpha = 2$ deg, b) $\alpha = 5$ deg, c) $\alpha = 7$ deg, and (d) $\alpha = 10$ deg. Vectors are subsampled by a factor of two in each dimension.

and Jacquin et al. [32] find that meander arises from turbulent fluctuations originating not in the freestream but, rather, in the shear layer as the vortex rolls up from the wing. Heyes et al. [28] are unable to conclude whether freestream turbulence or shear layer turbulence is responsible for vortex meander, or possibly a combination thereof.

Regardless of the source, vortex meander has been found to influence the mean measured properties of the vortex [10,26–28,33,34]. Devenport et al. [10] note that meander creates a smoothing effect that can make the vortex appear closer to the classically predicted structure, causing the mean vortex core to have a larger diameter and a reduced peak tangential velocity while creating apparent turbulent stresses [10,27,28,34]. The same effects were found by Westphal and Mehta [35] when forcing a low-frequency oscillation on a vortex generator.

In the present case, the typical vortex core meander distance at a downstream position of $x/c = 4.18$ is about $0.015c$ as found from the standard deviation of individual samples of the vorticity field derived from the PIV data, with no discernible preferential direction and a maximum meander distance of about $0.05c$. Though reported meander distances vary greatly, these results appear approximately consistent with other investigations [10,28–30], excepting Corsiglia et al. [26] who display motion nearly two orders of magnitude higher. Some studies find no significant meander at all [16,36].

Although freestream turbulence probably is a source of vortex meander in the present experiment, additional evidence suggests that it does not operate alone. Contributions from turbulence within the fin wake shear layer are possible, as Jacquin et al. [32] found, and the sequence of vector plots in Fig. 4 shows that wake fluid does spiral toward the vortex core. Additionally, the low-aspect-ratio fin places the trailing vortex in proximity to the test section wall, where it ingests turbulence from the wall boundary layer. It would be consistent with the findings of Jacquin et al. [32] and Heyes et al. [28] to suppose that this boundary-layer turbulence rolled up into the vortex would contribute to meander, and in fact, this supposition is confirmed by an experiment conducted in a boundary layer energized by low-profile vortex generators in which the meander distance increased by about 50% [37]. This result infers that vortex meander may be a phenomenon present in flight for missile geometries, not merely isolated to wind-tunnel studies, as the vortices produced by missile fins would entrain any turbulence found in the boundary layer growing on the missile body itself, analogous to the test section wall boundary layer in the present work. The influence of the nearby wall on vortex meander is one manner in which the development of a fin trailing vortex differs from that on an aircraft wing whose tip is much further distant from a wall.

The subject of vortex meander may be plumbed in much greater detail and is done so in a complementary paper [37]. As far as the present study is concerned, it is sufficient to note that significant meander is present, but the measured vortices are not corrected for the effect as in some other studies [10,28,34] (these corrections are found to be unnecessary in the present case, as discussed in [37]). In the earlier study of fin interaction aerodynamics [21], the balance measurements yield essentially time-averaged data, hence any meander of the impinging vortex would inherently be part of the force measurement. Given that the present investigation ought to be compatible with the associated aerodynamic data, it is therefore

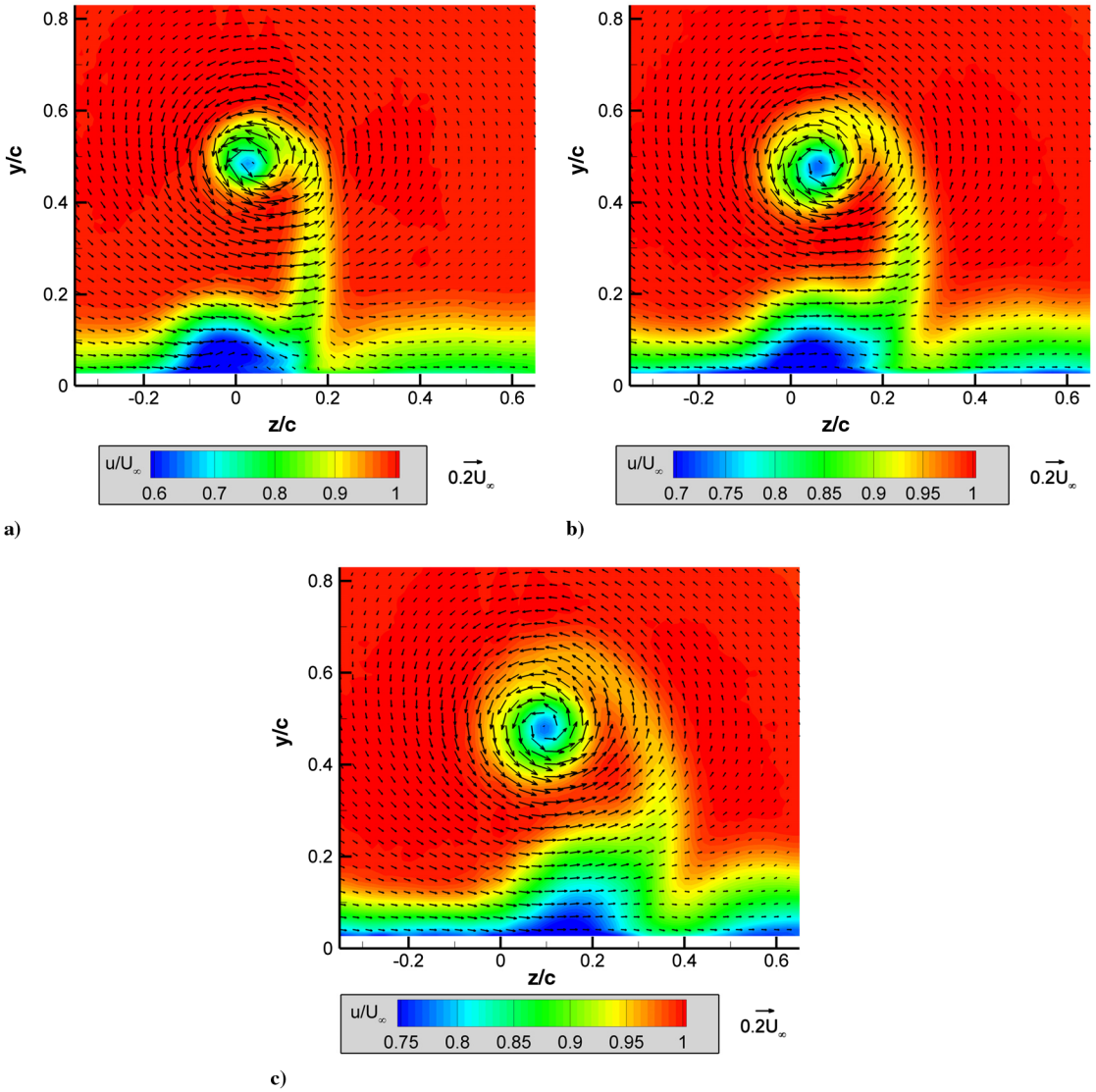

Fig. 4 Mean velocity fields at $M_\infty = 0.8$ and $\alpha = 10$ deg at varied distances from the trailing edge of the fin. a) $x/c = 0.51$, b) $x/c = 1.18$, and c) $x/c = 2.18$. Figure 3d provides the equivalent data for $x/c = 4.18$.

desirable to retain any effects of vortex meander in the analysis to follow.

Vortex Properties

Horizontal cuts of the tangential velocity v_θ through the center of the vortices shown in Figs. 3 and 4 are given in Fig. 5, where Fig. 5a provides curves for different fin angles at the downstream station $x/c = 4.18$ and Fig. 5b shows data for a constant α at differing x/c. These profiles are for $M_\infty = 0.8$; similar plots at four Mach numbers are shown in Fig. 5c to establish that normalized results are Mach number invariant. These data, as well as subsequent plots, are derived from 64×64 pixel interrogation window measurements, but essentially the same results were found from 32×32 pixel vectors only with greater noise. The velocity profiles represent the classical vortex structure of a small core delineated by peak velocities and further described by a linear velocity profile through the center of the core and an asymptotic decay back to quiescent freestream conditions [3]. Numerous experiments show the same structure (for example [7,8,10,11,18,26,38]). Despite the growth of the velocity magnitudes with increasing α (Fig. 5a) and the velocity decay with x/c (Fig. 5b), the basic structure is maintained.

The vortex properties may be reduced to singular values by defining the strength, size, and position of the vortex. The vortex strength is found from the circulation over some specified perimeter, then the vortex size and position readily follow from the area and centroid of that contour. Calculation of the required vorticity field is straightforward by finite differencing the velocity field, but several options are available to demarcate the vortex boundary over which to integrate the circulation. Definition of the vortex core has wide agreement in the open literature, where the contour is given by the point of maximum tangential velocity at each angular position, over which integration yields the vortex core circulation Γ_c; this corresponds to the maxima and minima of the profiles in Fig. 5. However, a quick examination of the velocity vectors in Figs. 3 and 4 demonstrates that this definition of the vortex core neglects a substantial portion of the vorticity, therefore it is desirable to define a second, larger vortex perimeter. The most common approach is that of Hoffmann and Joubert [39], where, by analogy with the 99%-velocity boundary-layer thickness, the contour is extended until the integration provides a circulation equivalent to 99% of the total circulation. In practice, however, this performs poorly in experimental data because measurement noise interferes with the integration long before the 99% boundary is reached, a difficulty noted in other experiments [13,26,39] and found to occur with the present data despite having averaged over a large number of individual PIV samples to obtain the clean appearance of Figs. 3 and 4. As such, the vortex is most confidently represented by its core properties.

Many previous investigations have demonstrated that the trailing vortex is asymmetric as it is shed from the fin or wing tip, and it does

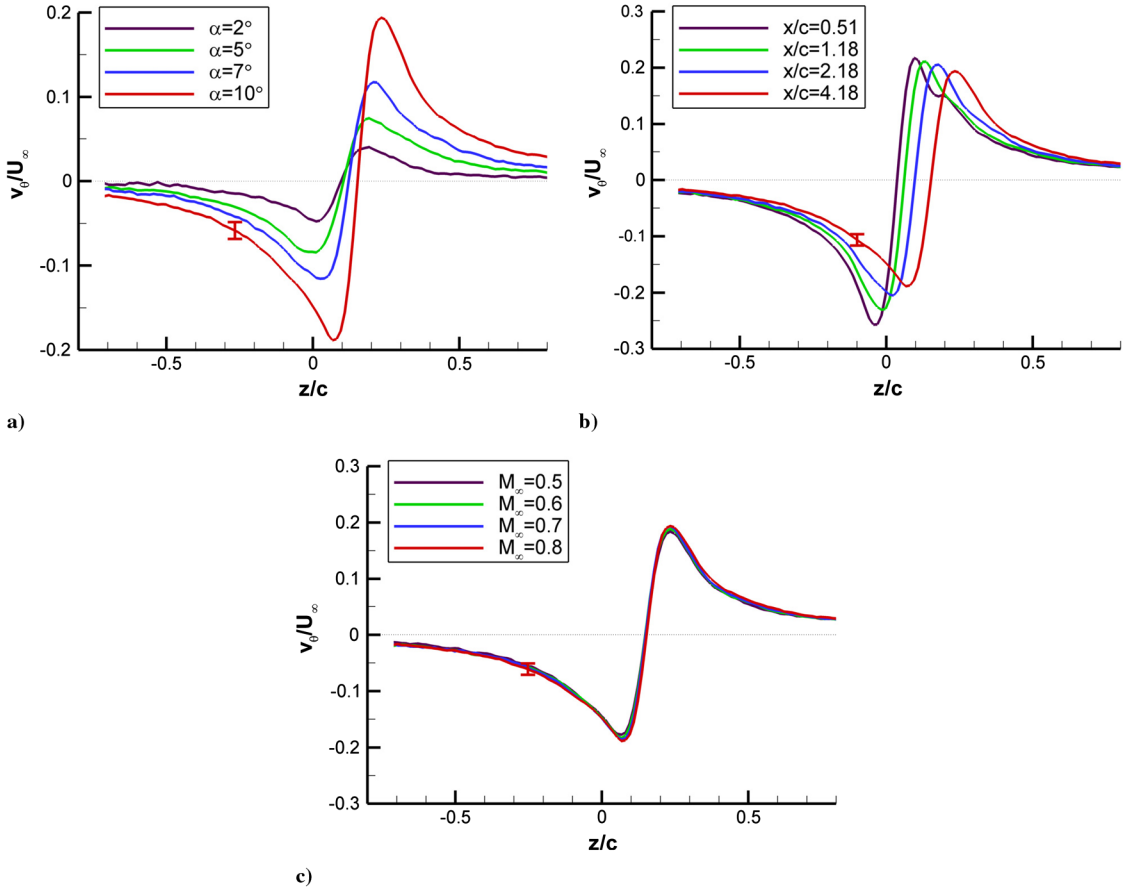

Fig. 5 Velocity profiles through the centers of the vortices shown in Figs. 3 and 4. a) Varying α at $x/c = 4.18$ and $M_\infty = 0.8$, b) varying x/c at $\alpha = 10$ deg and $M_\infty = 0.8$, and c) varying M_∞ at $x/c = 4.18$ and $\alpha = 10$ deg.

not become symmetric until some distance downstream [9,11–13,15,17,18,29,36,38]. The distance required to attain symmetry is widely variable with no obvious pattern. Gerontakos and Lee [36] find the vortex has become axisymmetric as rapidly as 0.625 chords downstream of the wing tip trailing edge; conversely, El-Ramly and Rainbird [9] and Zhang et al. [12] find symmetry has not been reached as far downstream as five chord lengths, as distant as their measurements extend. The most common result seems to find that the vortex has become symmetric, at least to within the measurement accuracy, at about 2 to 2.5 chord lengths downstream [15,17,29].

In the present case, the asymmetry of the vortex was examined by extracting velocity profiles radiating from the vortex center at different azimuthal angles, then finding the peak tangential velocity $v_{\theta,\max}$ and the distance at which it occurs (i.e., the local vortex core radius r_c). The results are shown in Fig. 6a for $\alpha = 10$ deg and $M_\infty = 0.8$ at the four different downstream stations. Angles are referenced from the positive horizontal axis, such that $\theta = 0$ deg extends in the $+z$ direction, with angles increasing counterclockwise. When $v_{\theta,\max}$ is considered, the vortex is distinctly asymmetric at $x/c = 0.51$ but gradually becomes less so with downstream distance until it is reasonably axisymmetric at $x/c = 4.18$. Conversely, the radius r_c shows no appreciable asymmetry within the noise of the measurement (perhaps a little asymmetry may be observed at $x/c = 0.51$). Given the broad range of past experiences concerning the point at which the vortex attains symmetry, for both long airfoils and low-aspect-ratio lifting surfaces, it is difficult to state whether the proximity of the wall has any influence. Higuchi et al. [38] specifically tested for this effect and detected no wall influence, and

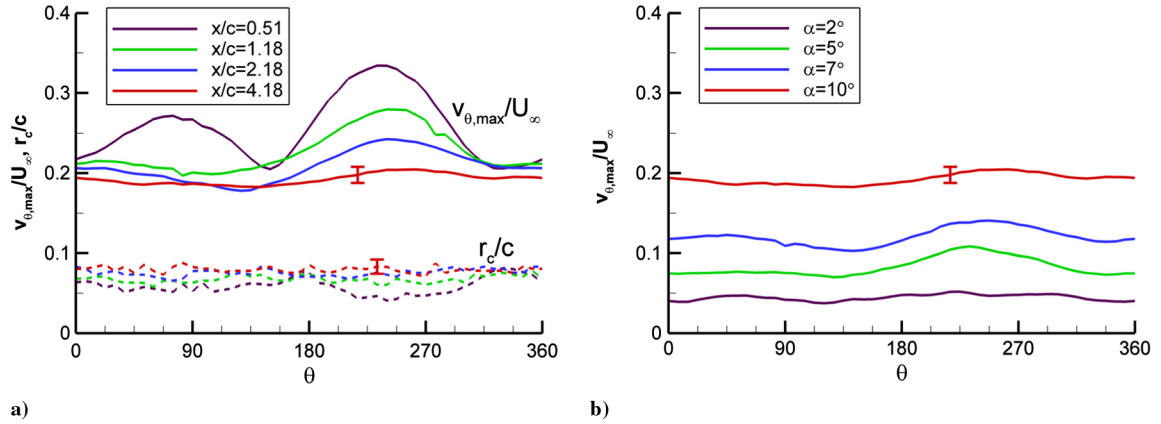

Fig. 6 Vortex asymmetry for a) $\alpha = 10$ deg and $M_\infty = 0.8$ and b) $x/c = 4.18$ and $M_\infty = 0.8$. Solid lines represent peak tangential velocity and broken lines represent the vortex core radius. Radius is given in a but not b.

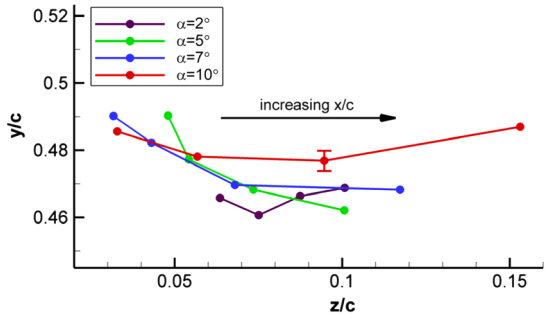

Fig. 7 Vortex trajectory as determined by the centroid of the vortex core.

similarly, Ramaprian and Zheng [17] showed no effect of the wall upon the vortex symmetry although it did influence the vortex trajectory (Chow et al. [16] also find a wall influence upon the trajectory, but make no study of the symmetry of the mean velocity field). Shekarriz et al. [13] note both an influence of the wall upon the vortex structure and a strong tangential velocity asymmetry but do not possess data that link the two observations.

The asymmetry observed in the peak tangential velocity but not matched by asymmetry in the vortex core radius appears counterintuitive but can be understood by recalling that during the roll-up process, vorticity is not conserved within the developing vortex core [10,40]. A vorticity flux exists across the boundary marked by the peak tangential velocity, with additional vorticity existing in the wake spiral drawn into the vortex core in the early stages of development. Evidently, this process does not occur symmetrically around the core, allowing the core radius to remain essentially constant.

Figure 6b provides $v_{\theta,\max}$ as a function of azimuthal angle for different values of α at $x/c = 4.18$ (core radii are omitted for clarity but are similar to those in Fig. 6a and show no significant asymmetry). Greater asymmetry is observed for the vortex at $\alpha = 5$ and 7 deg than at $\alpha = 2$ or 10 deg, suggesting that the downstream distance required for roll-up to complete is a complicated function of the initial vortex strength. This would help explain the range of distances reported in the literature, as might geometric differences.

The trajectory of a typical trailing vortex in flight is well known to descend from the tip of the lifting surface that generates it and move inboard as well [1–3]. However, wind-tunnel experiments have shown that, when using half-wing models, confinement within a test section appears to induce a rise to the trailing vortex once it leaves the tip without altering the inboard motion [6,16,33,36,41]. Ramaprian and Zheng [17] note that the vortex rise may actually be a lesser downward motion; this seems to be the case in the data of Shekarriz et al. [13] as well. In the present case, the vortex clearly moves laterally (z axis) away from the trailing edge regardless of its strength, as shown in Fig. 7 by tracking the position of the centroid of the vortex core; this is a descending direction relative to the fin. The vertical motion is not as definite, with data for $\alpha = 5$ and 7 deg displaying a clear inboard movement and data for $\alpha = 2$ and 10 deg first inboard, then outboard. The descent of the vortex does not correspond to prior wind-tunnel studies of various airfoil geometries, but the present data are insufficient to establish whether the proximity of the wall is responsible. It is conceivable that the relevant wall is actually the opposite wind-tunnel wall, which is nearer to the lifting surface in many prior experiments than it is here.

The key vortex parameters may be further examined for their dependence on downstream distance and fin angle of attack. The vortex core circulation Γ_c is found as detailed earlier and the core radius r_c is determined from the vortex core area assuming the core is circular, which Fig. 6 shows is reasonably accurate. The peak tangential velocity $v_{\theta,\max}$ cannot be assigned a single value because of the asymmetry in this parameter, and so the average value around the vortex core periphery is employed $v_{\theta,\max,\text{avg}}$. Figure 8 provides the results for these three quantities as a function of the downstream distance whereas Fig. 9 replots the same data as a function of the fin angle of attack. As Fig. 8 demonstrates, $v_{\theta,\max,\text{avg}}$ decays with downstream distance for all values of α whereas r_c generally increases; these trends roughly cancel each other when the circulation is computed, leaving Γ_c constant with downstream distance. A number of prior experiments have determined the same behavior for a variety of lifting surfaces [5–7,26] and others have found $v_{\theta,\max,\text{avg}}$ to decay

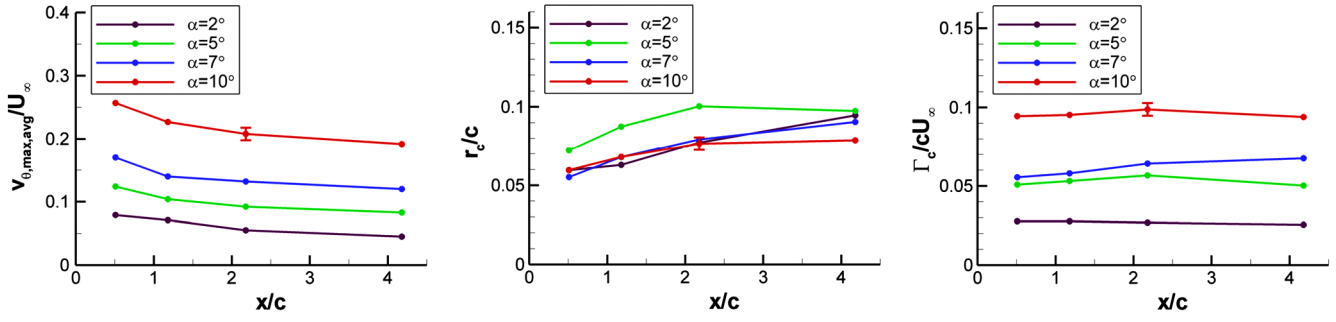

Fig. 8 Vortex properties as a function of downstream distance. a) Maximum tangential velocity, b) vortex core radius, and c) vortex core circulation.

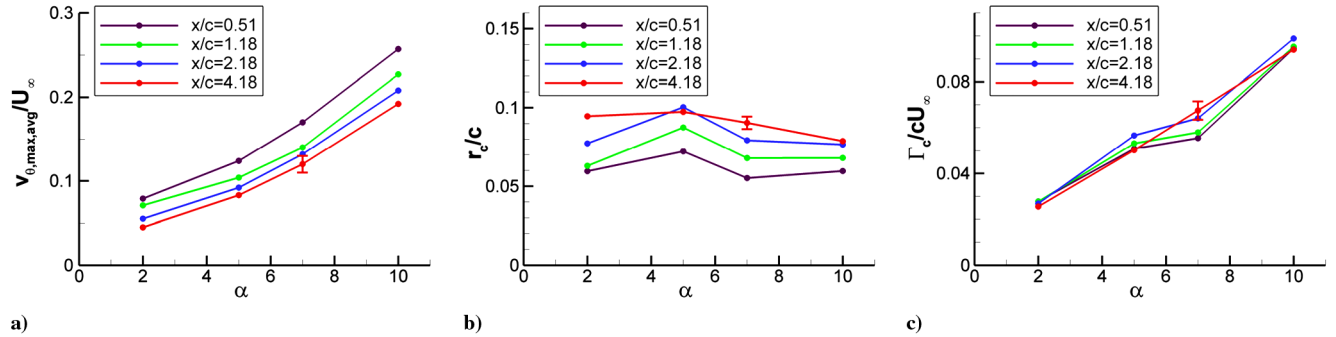

Fig. 9 Vortex properties as a function of fin angle of attack. a) Maximum tangential velocity, b) vortex core radius, and c) vortex core circulation.

although r_c and Γ_c both remain constant [11,36]. Still others find that a region of constant properties prevails for a large distance before $v_{\theta,\max,\text{avg}}$ begins to decay [8,17,42]. Brown's analytical approach [43] shows that for a vortex that exhibits self-similarity, $v_{\theta,\max,\text{avg}}$ can be expected to decay with downstream distance whereas r_c grows. Both [11,36] demonstrate self-similarity (as does the present work, revealed later in this document), and so it is not clear if the subtle growth of r_c may have been lost within measurement precision, explaining this aberrant behavior. Lezius [7] proposes that those experiments detecting a plateau region before the initiation of vortex decay are possible only in a low-turbulence environment such as tow tanks, explaining the relative rarity of this finding. This suggests that more rapid decay may be expected for vortices exposed to greater turbulence, and in fact Bailey et al. [33] find such a result.

The variation of vortex properties with the fin angle of attack, given in Fig. 9, shows that $v_{\theta,\max,\text{avg}}$ and Γ_c both increase considerably with α; r_c appears to diminish with α but these measurements are erratic enough to cloud such an observation. It is found in [6,11,44] that $v_{\theta,\max,\text{avg}}$ increases with α as in the present study, but they detect a linear relationship whereas Fig. 9a appears to show some curvature. Additionally, [6] determines that Γ_c increases linearly with α; Fig. 9c supports this finding only for $x/c = 4.18$. Perhaps not coincidentally, a considerably greater quantity of data was acquired at $x/c = 4.18$ than the other stations, suggesting experimental uncertainty may account for the nonlinear curves. The behavior of the vortex radius is even more confused; [6,26,36] show that r_c is approximately constant with α, but [7,11] find that r_c increases with α. Figure 9b supports neither, with a generally decreasing trend observed, though this really is only clear for the $x/c = 4.18$ data. Lezius [7] and Ciffone and Orloff [8] also indicate that a greater α leads to more rapid vortex decay, but this is not readily evident in the growth of r_c in Fig. 8b.

Axial Flow

The presence of axial flow in the vortex core is a crucial component of vortex behavior and interrelated with its rotation. Batchelor [45] demonstrated that changes in the rotational velocity of the vortex create a pressure gradient that will induce axial flow, and the nature of this flow is a direct predictor of the stability or decay of the vortex [3,44,46,47]. It has been well established that axial flow may occur in either direction within the vortex core (a velocity excess or a deficit) and appears to be dependent upon a wide variety of factors including the geometry of the lifting surface, its angle of attack, and downstream distance of the measurement [3,6,43–45,48]. Some studies have even noted a switch from a velocity excess to a deficit as the same vortex propagates downstream [29,47,49].

The axial velocities in the present experiment are shown in Fig. 10, complementary to the tangential velocities given in Fig. 5. In all cases, the axial velocity is found to be a deficit, regardless of vortex strength or downstream position, commonly denoted as wakelike flow. Figure 10a shows that stronger vortices produce a larger axial velocity deficit, whereas Fig. 10b shows the velocity deficit diminishing with downstream distance. The location of the peak deficit moves farther from the fin trailing edge in the z direction with both downstream distance and increasing vortex strength, consistent with the vortex trajectories plotted in Fig. 7. The small overshoot in v_x seen near the edge of the vortex core is not commonly found in the literature, but is not without precedent either [36,49,50]. As with the tangential velocity profiles in Fig. 5c, axial velocity profiles are found not to vary with Mach number; the plot is omitted due to triviality.

The axial velocity profiles in Fig. 10 all possess a second, minor peak due to the motion of the vortex entraining the low-speed fin wake shear layer as well as lifting the boundary-layer fluid from the wall, which is readily evident in Figs. 3 and 4 and suggests that turbulent fluid may be introduced into the vortex core. Such an effect is known to accelerate vortex decay [44,46] and potentially could explain differences with past studies that show an unchanging vortex for some distance downstream of the lifting surface without a nearby wall [8,42]. Freestream turbulence [33] or boundary-layer turbulence from the lifting surface itself [44] also can introduce turbulence into the vortex core and hasten decay. Evidence exists showing that larger values of α can be expected to create an axial velocity excess for which magnitude increases as α does [6,7,44,49], but the present measurements instead show a velocity deficit that grows with α. An escalated movement of low-speed wall boundary-layer fluid into the vortex core as the vortex strength rises may explain the inconsistency.

The axial velocity at its maximum deficit $v_{x,\max}$ and the radius of the region of velocity deficit r_x are provided in Figs. 11a and 11b respectively, where r_x is found from the full-width half-maximum of axial velocity profiles such as those in Fig. 10 (vertical profiles are used for this purpose rather than the horizontal profiles of Fig. 10 to avoid the influence of the second peak). At small values of α, the vortex often is ill defined and determination of both $v_{x,\max}$ and v_x can be problematic; for this reason, $\alpha = 2$ deg data are omitted from Fig. 11. Figure 11a indicates that the axial velocity deficit is greatest for larger fin angle of attack and diminishes with downstream distance in all cases, which was evident from Fig. 10. The width of the wake in Fig. 11b is more enlightening, showing that it increases with downstream distance as r_c was shown to do in Fig. 8b, and it is greater for smaller α, as the finding in Fig. 9b for r_c. The broadening of r_x with downstream distance is consistent with [8,50], but no comparative data were found regarding its dependence on α. Figure 11c presents the ratio of $v_{x,\max}$ to $v_{\theta,\max}$ and the ratio of r_x to r_c, both of which show that the axial and tangential properties differ near the fin trailing edge but come into closer agreement with downstream distance. This can be interpreted as requiring that vortex roll up be completed before axial and tangential properties behave similarly.

Vortex Similarity

Previous studies have suggested that additional normalization of the peak tangential velocity by the lift coefficient of the vortex

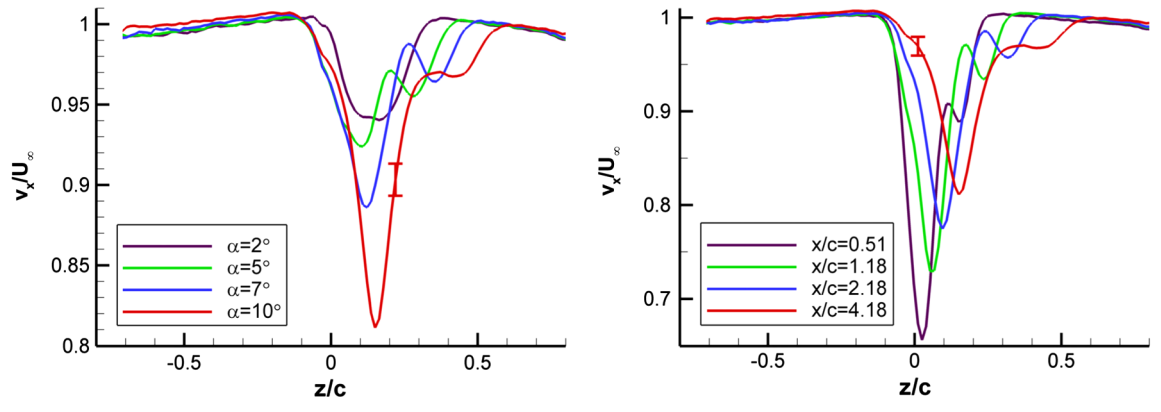

Fig. 10 Axial velocity profiles through the centers of the vortices shown in Figs. 3 and 4. a) Varying α at $x/c = 4.18$ and b) varying x/c at $\alpha = 10$ deg.

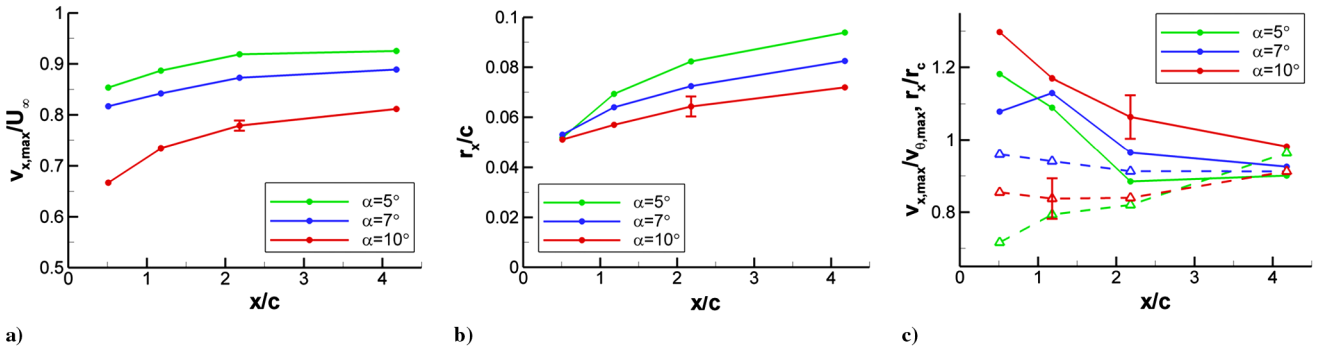

Fig. 11 Vortex axial properties as a function of downstream distance. a) Axial velocity at maximum deficit, b) vortex core radius, and (c) ratio of axial properties to tangential properties. Solid lines represent $v_{x,\max}/v_{\theta,\max}$ and broken lines represent r_x/r_c.

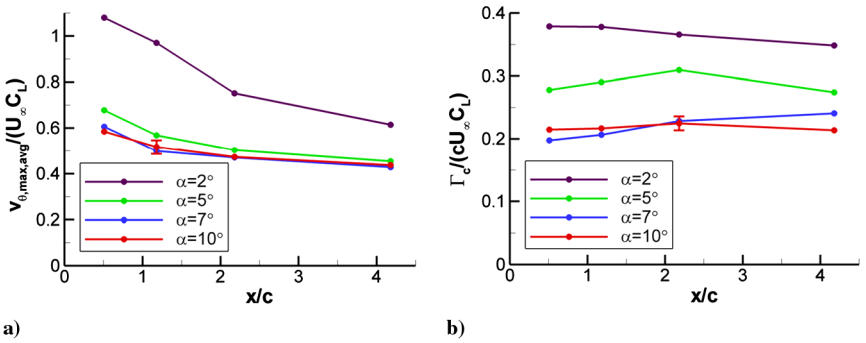

Fig. 12 Similarity of the vortex. a) Peak tangential velocity normalized by the fin lift coefficient and b) circulation normalized by the fin lift coefficient.

generator will produce similarity [5,26]. This proposition is examined in Fig. 12a, where values of the lift coefficient were obtained from the aerodynamic balance data concerning the same fin published in [21]. The plot shows that similarity is not particularly successful; although it may hold reasonably well for the strongest vortices, it performs poorly for $\alpha = 5$ deg and clearly not at all for $\alpha = 2$ deg. Other studies have provided data indicating that C_L is not a useful normalizer between different strength vortices [6,8], which coupled with Fig. 12a, question this attempt at similarity. In fact, Corsiglia et al. [26] suggest that this relationship is valid only for rectangular wings. Normalizing the vortex circulation by C_L is not successful either (Fig. 12b), which is noteworthy given the number of analyses that predict Γ_c based upon a linear relationship with the C_L of the lifting surface [43,51,52]. Although universality between vortex strengths cannot be shown, it already has been demonstrated in Fig. 8c that the vortex core circulation remains constant even as the vortex decays with downstream distance.

Although a convenient definition of the vortex boundary is given by the vortex core, the structure of a trailing vortex can be divided into multiple regions. Hoffmann and Joubert [39] predicted that the circulation distribution through the vortex would follow a second-order profile within the core and then transition to a logarithmic function of distance from the center. Numerous experiments have confirmed this behavior [5,11,17,26,37,40] and have added an outer region where roll-up effects may still be observed [11,26,36]. The analogy with the viscous sublayer and the log-law layer of a turbulent wall boundary layer is readily apparent.

Figure 13 shows the circulation through the trailing vortices as a function of the radial distance from the vortex center, normalized by the vortex core radius r_c and the core circulation Γ_c for each case, and plotted on semilogarithmic axes. Circulation values were computed by integrating the vorticity field at a sequence of concentric radii, symmetric about the vortex circumference. The data of Fig. 13a maintain a constant $x/c = 4.18$ while varying α, whereas Fig. 13b has constant $\alpha = 10$ deg and varies x/c. Clearly, the circulation profiles collapse excellently in the vortex core ($r/r_c < 1$) and display some minor deviation beyond this point. The data collapse establishes that vortex self-similarity exists between different fin angles of attack and at all four downstream stations despite the incomplete roll up; the differences in the outer region are possibly

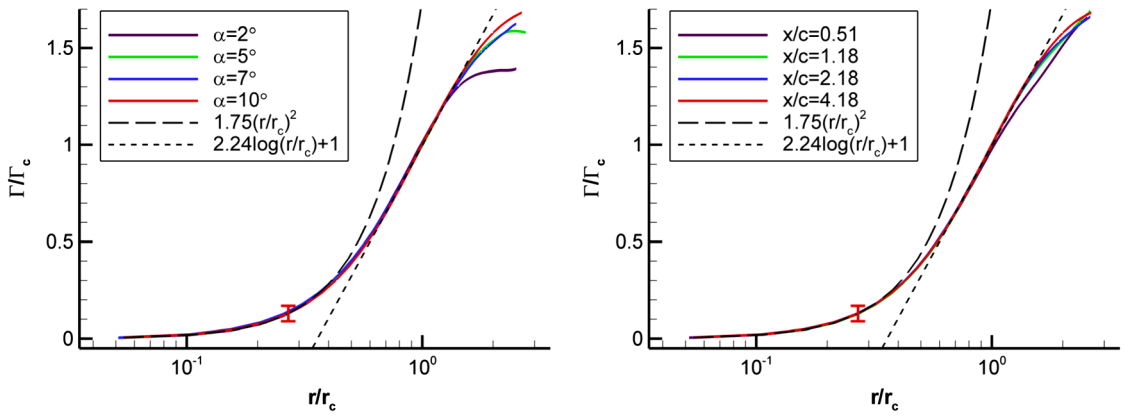

Fig. 13 Circulation profiles of the vortices shown in Figs. 3 and 4. a) Varying α at constant $x/c = 4.18$ and b) varying x/c at constant $\alpha = 10$ deg.

attributable to roll up. The plots also include curves for the expected second-order behavior within the core and the logarithmic behavior in the vicinity of the core boundary, with constants found by curve fitting and consistent with the range of values found in the literature [11,17,36,39]. In all cases, the fin trailing vortex well matches these second-order and logarithmic predictions, which, it should be noted, are nonintersecting.

Conclusions

A subscale experiment has been conducted to study the trailing vortex shed from a tapered fin installed on a wind-tunnel wall to represent missile configurations. Measurements have been acquired using stereoscopic particle image velocimetry in the cross plane to understand the behavior of the vortex that would impinge upon downstream control surfaces in a typical maneuvering missile configuration and to develop and validate computational models for simulating such interactions. Data were acquired at several different downstream locations behind the trailing edge of the fin but still within the near field of the flow, for multiple fin angles of attack and Mach numbers in the subsonic compressible regime.

The data show that the vortex strength increases markedly with upstream fin angle of attack, and data taken at progressively further stations following the fin trailing edge show the decay in vortex strength with downstream distance. No variation with Mach number can be discerned in the normalized velocity data within the range of Mach 0.5 to 0.8. The vortex core is defined by the locus of points marking the maximum tangential velocity of its rotation, which can be used to define the strength, size, and position of the vortex. This maximum tangential velocity is found to decay with downstream distance whereas the vortex radius increases, but these two effects counteract such that the vortex core circulation remains constant. Circulation and tangential velocity rise greatly as the fin angle of attack is increased, but the vortex radius is approximately constant or slightly decreasing. The vortex axial velocity is always a deficit, for which magnitude diminishes with downstream distance and smaller angle of attack.

Vortex roll up is observed to be largely complete by about four root chord lengths downstream of the fin trailing edge. Before this point, the vortex is strongly asymmetric in the maximum tangential velocity, but the vortex core radius remains nearly constant. This apparent inconsistency is attributed to a vorticity flux across the vortex core boundary during the roll-up process. The fin angle of attack is an additional parameter influencing the roll-up distance and the symmetry of the vortex. The rotational motion of the vortex is seen to draw low-speed turbulent fluid from the wind-tunnel wall boundary layer and the fin wake shear layer toward the vortex core, which appears to hasten the decay of the vortex and produce a larger axial velocity deficit than might be expected. Similar behavior would be anticipated on a missile configuration, with fin trailing vortices drawing fluid from the boundary layer that develops on the vehicle body and stands in contrast to a typical wingtip vortex.

The vortex exhibits self-similarity even within the roll-up region. The circulation profiles collapse to a single curve for all fin angles of attack and downstream stations when normalized by the local vortex core properties. The circulation distribution through the vortex follows a second-order profile within the core and then transitions to a logarithmic function of distance from the center, in concordance with the classical vortex structure. Attempts to normalize vortex properties such as circulation and radius by the fin's lift coefficient proved unsuccessful.

Acknowledgments

This work was supported by Sandia National Laboratories and the U.S. Department of Energy. Sandia is a multiprogram laboratory operated by Sandia Corporation, a Lockheed Martin Company, for the U.S. Department of Energy's National Nuclear Security Administration under contract DE-AC04-94AL85000. The authors would like to thank Walter P. Wolfe of Sandia National Laboratories for numerous fruitful discussions regarding fin aerodynamics and trailing vortices, Justin A. Smith of Sandia for measurements of the fin aerodynamics, and Thomas W. Grasser of Sandia for his contributions to the hardware design and fabrication.

References

[1] Lee, G. H., "Trailing Vortex Wakes," *Aeronautical Journal*, Vol. 79, No. 777, Sept. 1975, pp. 377–388.

[2] Hoeijmakers, H. W. M., "Vortex Wakes in Aerodynamics," *The Characterization and Modification of Wakes from Lifting Vehicles in Fluid*, AGARD CP-584 1996, pp. 1-1–1-12.

[3] Spalart, P. R., "Airplane Trailing Vortices," *Annual Review of Fluid Mechanics*, Vol. 30, 1998, pp. 107–138. doi:10.1146/annurev.fluid.30.1.107

[4] Jacquin, L., "On Trailing Vortices: A Short Review," *International Journal of Heat and Fluid Flow*, Vol. 26, No. 6, 2005, pp. 843–854. doi:10.1016/j.ijheatfluidflow.2005.10.001

[5] McCormick, B. W., Tangler, J. L., and Sherrier, H. E., "Structure of Trailing Vortices," *Journal of Aircraft*, Vol. 5, No. 3, 1968, pp. 260–267. doi:10.2514/3.43936

[6] Chigier, N. A., and Corsiglia, V. R., "Wind-Tunnel Studies of Wing Wake Turbulence," *Journal of Aircraft*, Vol. 9, No. 12, 1972, pp. 820–825. doi:10.2514/3.59082

[7] Lezius, D. K., "Water Tank Study of the Decay of Trailing Vortices," *AIAA Journal*, Vol. 12, No. 8, 1974, pp. 1065–1071. doi:10.2514/3.49412

[8] Ciffone, D. L., and Orloff, K. L., "Far-Field Wake-Vortex Characteristics of Wings," *Journal of Aircraft*, Vol. 12, No. 5, 1975, pp. 464–470.

[9] El-Ramly, Z., and Rainbird, W. J., "Flow Survey of the Vortex Wake Behind Wings," *Journal of Aircraft*, Vol. 14, No. 11, 1977, pp. 1102–1108. doi:10.2514/3.58897

[10] Devenport, W. J., Rife, M. C., Liapis, S. I., and Follin, G. J., "The Structure and Development of a Wing-Tip Vortex," *Journal of Fluid Mechanics*, Vol. 312, 1996, pp. 67–106. doi:10.1017/S0022112096001929

[11] Birch, D., Lee, T., Mokhtarian, F., and Kafyeke, F., "Structure and Induced Drag of a Tip Vortex," *Journal of Aircraft*, Vol. 41, No. 5, 2004, pp. 1138–1145. doi:10.2514/1.2707

[12] Zhang, H. J., Zhou, Y., and Whitelaw, J. H., "Near-Field Wing-Tip Vortices and Exponential Vortex Solution," *Journal of Aircraft*, Vol. 43, No. 2, 2006, pp. 445–449. doi:10.2514/1.15938

[13] Shekarriz, A., Fu, T. C., Katz, J., and Huang, T. T., "Near-Field Behavior of a Tip Vortex," *AIAA Journal*, Vol. 31, No. 1, 1993, pp. 112–118. doi:10.2514/3.11326

[14] Bridges, D. H., Blanton, J. N., Brewer, W. H., and Park, J. T., "Experimental Investigation of the Flow Past a Submarine at Angle of Drift," *AIAA Journal*, Vol. 41, No. 1, 2003, pp. 71–81. doi:10.2514/2.1915

[15] Stinebring, D. R., Farrell, K. J., and Billet, M. L., "The Structure of a Three-Dimensional Tip Vortex at High Reynolds Numbers," *Journal of Fluids Engineering: Transactions of the ASME*, Vol. 113, No. 3, 1991, pp. 496–503.

[16] Chow, J. S., Zilliac, G. G., and Bradshaw, P., "Mean and Turbulence Measurements in the Near Field of a Wingtip Vortex," *AIAA Journal*, Vol. 35, No. 10, 1997, pp. 1561–1567. doi:10.2514/2.1

[17] Ramaprian, B. R., and Zheng, Y., "Measurements in Rollup Region of the Tip Vortex from a Rectangular Wing," *AIAA Journal*, Vol. 35, No. 12, 1997, pp. 1837–1843. doi:10.2514/2.59

[18] Smart, M. K., Kalkhoran, I. M., and Bentson, J., "Measurements of Supersonic Wing Tip Vortices," *AIAA Journal*, Vol. 33, No. 10, 1995, pp. 1761–1768. doi:10.2514/3.12725

[19] Wang, F. Y., and Sforza, P. M., "Near-Field Experiments on Tip Vortices at Mach 3.1," *AIAA Journal*, Vol. 35, No. 4, 1997, pp. 750–753. doi:10.2514/2.172

[20] Milanovic, I. M., and Kalkhoran, I. M., "Near-Wake Measurements of a Delta Wing in a Supersonic Stream," *Journal of Aircraft*, Vol. 38, No. 2, 2001, pp. 315–325.

doi:10.2514/2.2764
[21] Beresh, S. J., Smith, J. A., Henfling, J. F., Grasser, T. W., and Spillers, R. W., "Interaction of a Fin Trailing Vortex with a Downstream Control Surface," *Journal of Spacecraft and Rockets* Vol. 46, No. 2, 2009. pp. 318–328.
doi:10.2514/1.40294
[22] Samimy, M., and Lele, S. K., "Motion of Particles with Inertia in a Compressible Free Shear Layer," *Physics of Fluids A*, Vol. 3, No. 8, 1991, pp. 1915–1923.
doi:10.1063/1.857921
[23] Melling, A., "Tracer Particles and Seeding for Particle Image Velocimetry," *Measurement Science and Technology*, Vol. 8, No. 12, 1997, pp. 1406–1416.
doi:10.1088/0957-0233/8/12/005
[24] Soloff, S. M., Adrian, R. J., and Liu, Z.-C., "Distortion Compensation for Generalized Stereoscopic Particle Image Velocimetry," *Measurement Science and Technology*, Vol. 8, No. 12, 1997, pp. 1441–1454.
doi:10.1088/0957-0233/8/12/008
[25] Beresh, S. J., Henfling, J. F., Erven, R. J., and Spillers, R. W., "Penetration of a Transverse Supersonic Jet into a Subsonic Compressible Crossflow," *AIAA Journal*, Vol. 43, No. 2, 2005, pp. 379–389.
doi:10.2514/1.9919
[26] Corsiglia, V. R., Schwind, R. G., and Chigier, N. A., "Rapid Scanning, Three-Dimensional Hot-Wire Anemometer Surveys of Wing-Tip Vortices," *Journal of Aircraft*, Vol. 10, No. 12, 1973, pp. 752–757.
doi:10.2514/3.60301
[27] Baker, G. R., Barker, S. J., Bofah, K. K., and Saffman, P. G., "Laser Anemometer Measurements of Trailing Vortices in Water," *Journal of Fluid Mechanics*, Vol. 65, Part 2, 1974, pp. 325–336.
doi:10.1017/S0022112074001418
[28] Heyes, A. L., Jones, R. F., and Smith, D. A. R., "Wandering of Wing-Tip Vortices," *Proceedings of the 12th International Symposium on Applications of Laser Techniques to Fluid Mechanics*, Paper 35-3, Lisbon, Portugal, 2004.
[29] Green, S. I., and Acosta, A. J., "Unsteady Flow in Trailing Vortices," *Journal of Fluid Mechanics*, Vol. 227, 1991, pp. 107–134.
doi:10.1017/S0022112091000058
[30] Yeung, A. F. K., and Lee, B. H. K., "Particle Image Velocimetry Study of Wing-Tip Vortices," *Journal of Aircraft*, Vol. 36, No. 2, 1999, pp. 482–484.
doi:10.2514/2.2460
[31] Rokhsaz, K., Foster, S. R., and Miller, L. S., "Exploratory Study of Aircraft Wake Vortex Filaments in a Water Tunnel," *Journal of Aircraft*, Vol. 37, No. 6, 2000, pp. 1022–1027.
doi:10.2514/2.2706
[32] Jacquin, L., Fabre, D., Geffroy, P., and Coustols, E., "The Properties of a Transport Aircraft Wake in the Extended Near Field: an Experimental Study," AIAA Paper 2001-1038, Jan. 2001.
[33] Bailey, S. C. C., Tavoularis, S., and Lee, B. H. K., "Effects of Freestream Turbulence on Wing-Tip Vortex Formulation and Near Field," *Journal of Aircraft*, Vol. 43, No. 5, 2006, pp. 1282–1291.
doi:10.2514/1.19433
[34] Bailey, S. C. C., and Tavoularis, S., "Measurements of the Velocity Field of a Wing-Tip Vortex, Wandering in Grid Turbulence," *Journal of Fluid Mechanics*, Vol. 601, 2008, pp. 281–315.
[35] Westphal, R. V., and Mehta, R. D., "Interaction of an Oscillating Vortex with a Turbulent Boundary Layer," *Experiments in Fluids*, Vol. 7, No. 6, 1989, pp. 405–411.
[36] Gerontakos, P., and Lee, T., "Near-Field Tip Vortex Behind a Swept Wing Model," *Experiments in Fluids*, Vol. 40, No. 1, 2006, pp. 141–155.
doi:10.1007/s00348-005-0056-y
[37] Beresh, S. J., Henfling, J. F., and Spillers, R. W., "Meander of a Fin Trailing Vortex Measured Using Particle Image Velocimetry," AIAA Paper 2009-0406, Jan. 2009.
[38] Higuchi, H., Quadrelli, J. C., and Farell, C., "Vortex Roll-Up from an Elliptic Wing at Moderately Low Reynolds Numbers," *AIAA Journal*, Vol. 25, No. 12, 1987, pp. 1537–1542.
doi:10.2514/3.9821
[39] Hoffmann, E. R., and Joubert, P. N., "Turbulent Line Vortices," *Journal of Fluid Mechanics*, Vol. 16, No. 3, 1963, pp. 395–411.
doi:10.1017/S0022112063000859
[40] Phillips, W. R. C., "The Turbulent Trailing Vortex During Roll-up," *Journal of Fluid Mechanics*, Vol. 105, 1981, pp. 451–467.
doi:10.1017/S0022112081003285
[41] Lombardi, G., and Skinner, P., "Wing-Tip Vortex in the Near Field: An Experimental Study," *Journal of Aircraft*, Vol. 42, No. 5, 2005, pp. 1366–68.
[42] Iversen, J. D., "Correlation of Turbulent Trailing Vortex Decay Data," *Journal of Aircraft*, Vol. 13, No. 5, 1976, pp. 338–342.
doi:10.2514/3.44529
[43] Brown, C. E., "Aerodynamics of Wake Vortices," *AIAA Journal*, Vol. 11, No. 4, 1973, pp. 531–536.
doi:10.2514/3.6781
[44] Orloff, K. L., "Trailing Vortex Wind-Tunnel Diagnostics with a Laser Velocimeter," *Journal of Aircraft*, Vol. 11, No. 8, 1974, pp. 477–482.
doi:10.2514/3.60371
[45] Batchelor, G. K., "Axial Flow in Trailing Line Vortices," *Journal of Fluid Mechanics*, Vol. 20, Part 4, 1964, pp. 645–658.
doi:10.1017/S0022112064001446
[46] Phillips, W. R. C., and Graham, J. A. H., "Reynolds-Stress Measurements in a Turbulent Trailing Vortex," *Journal of Fluid Mechanics*, Vol. 147, 1984, pp. 353–371.
doi:10.1017/S0022112084002123
[47] Singh, P. I., and Uberoi, M. S., "Experiments on Vortex Stability," *Physics of Fluids*, Vol. 19, No. 12, 1976, pp. 1858–1863.
[48] Anderson, E. A., and Lawton, T. A., "Correlation Between Vortex Strength and Axial Velocity in a Trailing Vortex," *Journal of Aircraft*, Vol. 40, No. 4, 2003, pp. 699–704.
doi:10.2514/2.3148
[49] Thompson, D. H., "Experimental Study of Axial Flow in Wing Tip Vortices," *Journal of Aircraft*, Vol. 12, No. 11, 1975, pp. 910–911.
doi:10.2514/3.44500
[50] Logan, A. H., "Vortex Velocity Distributions at Large Downstream Distances," *Journal of Aircraft*, Vol. 8, No. 11, 1971, pp. 930–932.
doi:10.2514/3.44313
[51] Nielsen, J. N., *Missile Aerodynamics*, McGraw–Hill, New York, 1960, p. 152.
[52] Rule, J. A., and Bliss, D. B., "Prediction of Viscous Trailing Vortex Structure from Basic Loading Parameters," *AIAA Journal*, Vol. 36, No. 2, 1998, pp. 208–218.
doi:10.2514/2.7503

F. Coton
Associate Editor